Monthly Notices
of the
ROYAL ASTRONOMICAL SOCIETY

MNRAS **459,** 2097–2105 (2016)
Advance Access publication 2016 April 6

doi:10.1093/mnras/stw693

Evidence for variable, correlated X-ray and optical/IR extinction towards the nearby, pre-main-sequence binary TWA 30

David A. Principe,[1,2,3★] G. Sacco,[4★] J. H. Kastner,[3★] B. Stelzer[5] and J. M. Alcalá[6]

[1]*Núcleo de Astronomía de la Facultad de Ingeniería, Universidad Diego Portales, Av. Ejército Libertador 441, Santiago 8320000, Chile*
[2]*Millennium Nucleus Protoplanetary Disks, Universidad Diego Portales, Av. Ejército Libertador 441, Santiago 8320000, Chile*
[3]*Laboratory for Multiwavelength Astrophysics, Rochester Institute of Technology (RIT), 1 Lomb Memorial Dr., Rochester, NY 14623, USA*
[4]*INAF – Osservatorio Astrofisico di Arcetri, Largo E. Fermi 5, I-50125 Firenze, Italy*
[5]*INAF – Osservatorio Astronomico di Palermo, Piazza del Parlamento 1, I-90134 Palermo, Italy*
[6]*INAF – Osservatorio Astronomico di Capodimonte, via Moiariello 16, I-80131 Napoli, Italy*

Accepted 2016 March 22. Received 2016 March 21; in original form 2015 June 8

ABSTRACT

We present contemporaneous *XMM–Newton* X-ray and ground-based optical/near-IR spectroscopic observations of the nearby ($D \approx 42$ pc), low-mass (mid-M) binary system TWA 30A and 30B. The components of this wide (separation ∼3400 au) binary are notable for their nearly edge-on disc viewing geometries, high levels of variability, and evidence for collimated stellar outflows. We obtained *XMM–Newton* X-ray observations of TWA 30A and 30B in 2011 June and July, accompanied (respectively) by Infrared Telescope Facility SpeX (near-IR) and VLT XSHOOTER (visible/near-IR) spectroscopy obtained within ∼20 h of the X-ray observations. TWA 30A was detected in both *XMM–Newton* observations at relatively faint intrinsic X-ray luminosities ($L_X \sim 8 \times 10^{27}$ erg s^{-1}) compared to stars of similar mass and age. The intrinsic (0.15–2.0 keV) X-ray luminosities measured in 2011 had decreased by a factor 20–100 relative to a 1990 (*ROSAT*) X-ray detection. TWA 30B was not detected, and we infer an upper limit on its X-ray Luminosity of $L_X \lesssim 3.0 \times 10^{27}$ erg s^{-1}. We measured a decrease in visual extinction towards TWA 30A (from $A_V \approx 14.9$ to $A_V \approx 4.7$) between the two 2011 observing epochs, and we find evidence for a corresponding significant decrease in X-ray absorbing column (N_H). The apparent correlated change in A_V and N_H is suggestive of variable obscuration of the stellar photosphere by disc material composed of both gas and dust. However, in both observations, the inferred N_H to A_V ratio is lower than that typical of the interstellar medium, suggesting that the disc is either depleted of gas or is deficient in metals in the gas phase.

Key words: magnetic fields – protoplanetary discs – circumstellar matter – stars: low-mass – stars: pre-main-sequence – stars: variables: T Tauri, Herbig Ae/Be.

1 INTRODUCTION

Contemporaneous multiwavelength observations of nearby pre-main-sequence (pre-MS) stars provide opportunities to investigate variable astrophysical phenomena related to interactions between such stars and their planet-forming circumstellar discs, as well as to measure the gas and dust content of these discs. Pre-MS stars $\leq$2 M$_\odot$ (i.e. T Tauri stars) are broadly subdivided into classical T Tauri stars (cTTSs) and weak-lined T Tauri stars (wTTSs) based on the strength of their Hα emission, which serves as a proxy for their stage of evolution as star–disc systems. During the cTTS (strong Hα emission) stage, the pre-MS star is orbited by an optically thick circumstellar disc from which the star is actively accreting via magnetospheric accretion processes (Koenigl 1991; Shu et al. 1994). Eventually, the circumstellar gas disc dissipates (via photoevaporation, planet formation, and/or viscous evolution; e.g. Lubow & D'Angelo 2006; Ciesla 2007; Gorti & Hollenbach 2009; Zhu et al. 2012), the accretion process halts, and the pre-MS star enters the wTTS (weak Hα emission) phase of evolution. As discussed in Williams & Cieza (2011, and reference therein), the median disc lifetime for pre-MS stars (i.e. the length of the cTTS phase) is ∼ 3 Myr, although disc dissipation times for any individual system vary widely (i.e. ∼1–10 Myr). Therefore, pre-MS stars with circumstellar discs $\gtrsim$8 Myr provide a unique opportunity to investigate late-stage disc evolution.

Near-infrared (IR), optical and X-ray variability has been characterized in many pre-MS star–disc systems and is the likely result of star–disc interactions (e.g. magnetospheric accretion,

★E-mail: daveprincipe1@gmail.com (DAP); gsacco@arcetri.inaf.it (GS); jhkpci@cis.rit.edu (JHK)

© 2016 The Authors
Published by Oxford University Press on behalf of the Royal Astronomical Society

Downloaded from https://academic.oup.com/mnras/article-abstract/459/2/2097/2595075 by guest on 21 April 2020

disc warps and/or clumps, winds, hotspots; Schisano et al. 2009; Flaherty & Muzerolle 2010; Bouvier et al. 2007; Principe et al. 2014). The variability time-scale will depend on the mechanism producing such variability and can range anywhere from hours to years. Moreover, some of these variability mechanisms are dependent on the orientation of the star–disc system with respect to our line of sight. Previous studies of nearly edge-on or highly inclined circumstellar discs confirm the presence of variability associated with the temporary and/or periodic obscuration of the stellar photosphere from disc warps/and or clumps (e.g. AA Tau, RY Lupi, T Cha; Bouvier et al. 2003; Grosso et al. 2007; Manset et al. 2009; Schisano et al. 2009). Such photospheric obscuration would only be expected to be observed in highly inclined discs, because the bulk of circumstellar material is confined to the disc plane. Contemporaneous multiwavelength observations can elucidate this mechanism of variability in star–disc systems.

More generally, multiwavelength studies of nearby ($\lesssim$100 pc), pre-MS M stars provide the opportunity to investigate the early evolution of the most plentiful type of star in the Galaxy (Lépine et al. 2013, and ref. therein). High-energy radiation (e.g. NUV, FUV, and X-ray) from nearby M-type stars decreases with increasing age, as Stelzer et al. (2013) demonstrated by comparing the high-energy luminosities of early M-type pre-MS stars in the TW Hydrae Association (TWA; age $\sim$8 Myr) with those of a nearby ($<$10 pc) main-sequence M dwarf sample. However, the time-scale for this decline is not well determined, especially for mid- to late-M stars. Moreover, constraints on high-energy emission and variability are particularly important for theories of planet formation around M-type stars, given that their habitable zones lie at relatively small orbital radii and that such radiation can have important effects on the evaporation and chemistry of protoplanetary discs and planetary atmospheres (Lammer et al. 2003; Segura et al. 2005; Tarter et al. 2007; Chadney et al. 2015; Gorti, Hollenbach & Dullemond 2015).

The two components of the recently discovered wide separation binary ($\sim$3400 au) TWA 30 (Looper et al. 2010a,b) represent two of the nearest examples of actively accreting, M-type pre-MS star–disc systems ($d \sim 42$ pc). TWA 30A and 30B are members of the $\sim$8 Myr-old TWA, one of the nearest comoving groups of pre-MS stars to Earth (Kastner et al. 1997; Mamajek, Meyer & Liebert 2002; Ducourant et al. 2014). Members of the TWA have been extensively studied (e.g. TW Hya and Hen 3-600; Jayawardhana et al. 1999; Krist et al. 2000; Kastner et al. 2002; Huenemoerder et al. 2007; Rodriguez et al. 2015) because their proximity and age makes them ideal objects for the study of protoplanetary systems which form in the first $\sim$1–10 Myr. Furthermore, the proximity of the TWA allows for easier characterization of very low-mass stars like TWA 30A (M5) and 30B (M4) since stars of such late spectral types would be too faint for detailed study at the $>$100 pc distances typical of well-studied star-forming clouds.

Both TWA 30A and 30B have mid-IR excesses indicative of dusty circumstellar discs (Schneider, Melis & Song 2012) and both display signatures of outflows and jet emission in the form of strong forbidden emission lines (e.g. [O I], [O II], [N II], and [Si II]). These lines display small velocity shifts with respect to rest velocity, suggesting that the outflows lie nearly perpendicular to the line of sight. If the outflows are perpendicular to the circumstellar disc, then this orientation suggests that the viewing geometry of these relatively rare late-stage (i.e. evolved $\sim$8 Myr) discs around TWA 30A and 30B are nearly edge-on (Looper et al. 2010a,b). The nearby TWA 30A and 30B systems hence offer the potential to study both gas and dust absorption and emission, respectively, by measuring the attenuation of coronally and/or accretion generated X-rays by circumstellar gas and the attenuation and reprocessing of photospheric near-IR and optical emission by circumstellar dust, with little or no contamination from interstellar material. Both TWA 30A and 30B display significant near-IR variability (Looper et al. 2010a,b), although the mechanisms causing the variability in these stars appear to be different. The near-IR variability of TWA 30A tends to follow the reddening vector, with typical values in the range of $A_V \sim 1$–9. This suggests that a changing column density of circumstellar disc dust is responsible for variable reddening of the stellar photosphere. In contrast, the near-IR variability of 30B tends to follow the CTTS locus, possibly indicative of reprocessed starlight emitted by an inner-disc structure and variably scattered towards us.

Table 1. TWA 30 observations.

Object	Obs.date (UTC)	Telescope	Exposure (s)
TWA 30A	2011-06-07 10:40:52	XMM-EPIC	13950[a]/–/–
TWA 30A	2011-06-08 05:53:04	IRTF-SpeX	1440
TWA 30A	2011-07-15 00:00:07	VLT-XSHOOTER	920/560/600[b]
TWA 30A	2011-07-15 21:59:40	XMM-EPIC	14720[a]/21290/21320
TWA 30B	2011-06-07 10:40:52	XMM-EPIC	13950[a]/–/–
TWA 30B	2011-06-08 06:35:21	IRTF-SpeX	750
TWA 30B	2011-07-15 00:38:27	VLT-XSHOOTER	1960/1600/1160[b]
TWA 30B	2011-07-15 21:59:40	XMM-EPIC	14720[a]/21290/21320

[a]Effective exposure times (pn/MOS1/MOS2) due to interruption by background flaring events.
[b]Exposure time for each spectrograph arm in the format of UVB, VIS, and NIR.

TWA 30A was reported in Looper et al. (2010a) to have a counterpart in X-rays in the *ROSAT* All Sky Survey (RASS) Faint Source Catalogue at a distance of 17.6 arcsecond from the 2MASS position, well within the $\sim$25 arcsecond spatial resolution of *ROSAT* at $\sim$1 keV. TWA 30B was not detected in RASS. X-rays in pre-MS stars can be coronally generated and/or the result of star–disc interactions (e.g. star-disc magnetic reconnection events and magnetically funnelled accretion) and have been shown to be variable on time-scales of hours to years (Bouvier et al. 2007; Principe et al. 2014). Therefore, X-ray observations of such stars and their X-ray variability offer a means to probe pre-MS stellar magnetic and accretion activity. Furthermore, soft ($<$1 keV) X-ray emission is absorbed by circumstellar gas (mainly atomic C, N, and O; Wilms, Allen & McCray 2000) and can thus be used to estimate a line of sight gas column density due to the disc. X-ray (and UV) emission is also an important source of disc ionization and chemistry in protoplanetary discs (Glassgold, Galli & Padovani 2012). X-ray (and UV) heating can alter the disc structure by heating the surface layers of the disc resulting in a 'flared disc' (Meijerink et al. 2012).

To investigate the nature, origins, and variability of the X-ray emission from TWA 30A and 30B, we have obtained near-simultaneous X-ray and near-IR spectroscopy of these two systems. We present the observations in Section 2. We discuss results in Sections 3 and 4 and present our summary and conclusions in Section 5.

2 OBSERVATIONS

2.1 X-rays

X-ray observations of TWA 30A and 30B (Table 1) were obtained with the European Photon Imaging Camera (EPIC) instrument on board the *XMM–Newton* Observatory (Obs.IDs 0672500201 and 0672500301). Two $\sim$25 ks exposures were obtained near

Downloaded from https://academic.oup.com/mnras/article-abstract/459/2/2097/2595075 by guest on 21 April 2020

simultaneously with Very Large Telescope (VLT) and Infrared Telescope Facility (IRTF) observations (Section 2.2), respectively. All observations were reduced using the ESA XMM Science Analysis System (SAS) version 11.0. Observations with the EPIC instrument include both the pn and the two MOS cameras. Observations using all three detectors have been energy filtered (0.15–10 keV) and time filtered for flaring particle background. The *XMM–Newton* observation obtained in 2011 June was contaminated by a large solar flaring event ∼15 ks into the observation. In order to extract data from this observation, the EPIC-pn event files were time filtered such that only the data during the first ∼15 ks were used. EPIC-MOS1 and MOS2 data from the 2011 June epoch were not used due to poor quality from the flaring particle background. A small background flaring event (∼5 ks) was time filtered from the 2011 July observation. The resulting effective useful exposure times for the EPIC observations are listed in Table 1. Standard XMM-SAS tasks were used to extract spectral files as well as region statistics, including source count rates and background count rate estimates at the positions of TWA 30A and 30B in both observations. Source extraction regions were circles with radii of ∼15 arcsec centred at the 2MASS position of TWA 30A and 30B, and background extraction regions were circles with radii of ∼50 arcsec positioned nearby TWA 30A and 30B on the same chip with no clear point sources or extended emission contaminants.

2.2 Near-IR and optical

Near-IR/optical spectroscopy of TWA 30A and 30B was obtained in 2011 June and 2011 July with the 3.0 m IRTF and the 8.2 m VLT, respectively. These observations were intended to obtain near-IR spectroscopic data contemporaneous with the XMM observations described in section 2.1. Near-IR spectroscopy of TWA 30A and 30B were obtained using the medium resolution Spectrograph and Imager (SpeX) on the IRTF. Observations of TWA 30A were obtained in cross-dispersed mode (SXD) with a 0.5 arcsec slit resulting in a resolution of ∼1200. TWA 30B observations were obtained in prism mode with a 0.5 arcsec slit resulting in a resolution of ∼120. The IRTF SpeX data were reduced and combined using Spextool.[1] Near-IR, optical, and UV spectra of TWA 30A and 30B were obtained using the X-SHOOTER instrument on the VLT (Program 287.C-5039) in nodding mode with slit widths of 0.8, 0.9, and 0.9 arcsec with corresponding resolutions of ∼6200, 8800, and 5300 for the UVB, VIS, and NIR arms, respectively. Basic data reduction was performed using the X-SHOOTER pipeline and the subsequent telluric correction and NIR response function were applied with IRAF. More details of the XSHOOTER data reduction can be found in Alcalá et al. (2014). Details of the observations presented here are provided in Table 1.

3 RESULTS

3.1 Near-IR and Optical Spectroscopy

Reduced spectra of TWA 30A and 30B from Looper et al. (2010a,b) were provided by D. Looper and compared to the more recent IRTF and VLT observations presented in this work (Section 2.2; Figs 1 and 2). In the case of TWA 30A, the continuum shapes at wavelengths $\gtrsim$1.5 μm during the 2011 June and July epochs are similar to those of the most and least reddened spectra presented in Looper et al. (2010a), respectively (Fig. 1). We note that the TWA 30A spectra from the 2011 June and July epochs are flatter in the *J*-band region than the spectra displayed in Looper et al. (2010a). In contrast to the 2011 June/July continuum shape change in TWA 30A, both TWA 30B spectra appear to closely resemble those in Looper et al. (2010b) that were obtained during periods, where this object displayed minimal near-IR excess (Fig. 2). The comparison between previous near-IR spectroscopy and the near-IR spectra, we obtained, is discussed further in Section 4.

Standard broad-band near-IR (*JHK*) photometry were extracted from the 2011 June and July IRTF and VLT spectra using standard 2MASS *JHK* filter bandpasses (Cohen, Wheaton & Megeath 2003). A custom IDL program was used to integrate spectral flux

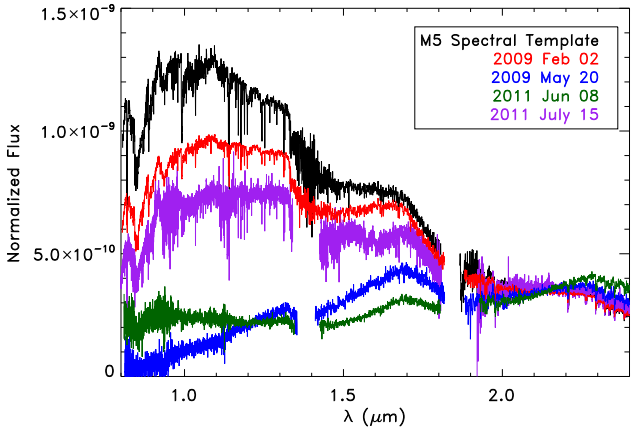


Figure 1. Two extreme examples of the TWA 30A near-IR SpeX spectra originally presented in Looper et al. (2010b) compared to 2011 June and 2011 July SpeX (green) and VLT (purple) observations presented in this work. An unreddened M5 spectral template is shown in black. All spectra have been normalized to the flux at ∼2.15 μm. Spectra from top to bottom at 1 μm are: M5 spectral template; 2009 Feb 02; 2011 July 15; 2011 Jun 08; and 2009 May 20.

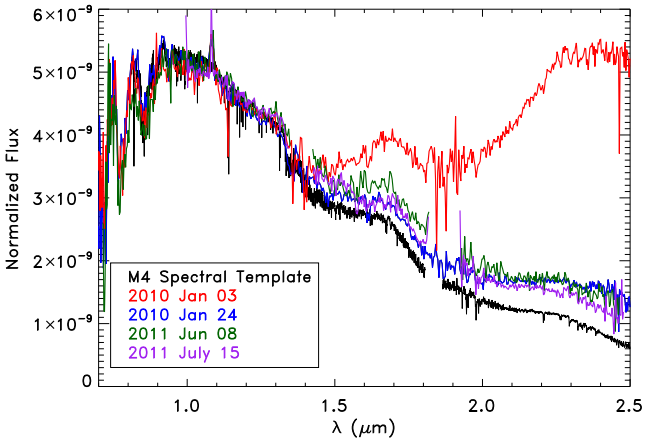


Figure 2. Two extreme examples of TWA 30B SpeX observations originally presented in Looper et al. (2010a) exhibiting high and low levels of disc excess compared to an unreddened M4 spectral template (black) and 2011 June and 2011 July SpeX (green) and VLT (purple) observations presented in this work. The VLT spectrum of TWA 30B has been rebinned to match the resolution of the IRTF SpeX spectra. All spectra have been normalized to the flux at ∼1.27 μm. The spectra at epochs 2010 Jan 24, 2011 Jun 08, and 2011 July 15 are nearly coincident.

[1] http://irtfweb.ifa.hawaii.edu/∼spex/Spextool_v3.4.txt and a custom IDL code by D. Looper following methods described in detail in Looper et al. (2010a,b).

Downloaded from https://academic.oup.com/mnras/article-abstract/459/2/2097/2595075 by guest on 21 April 2020

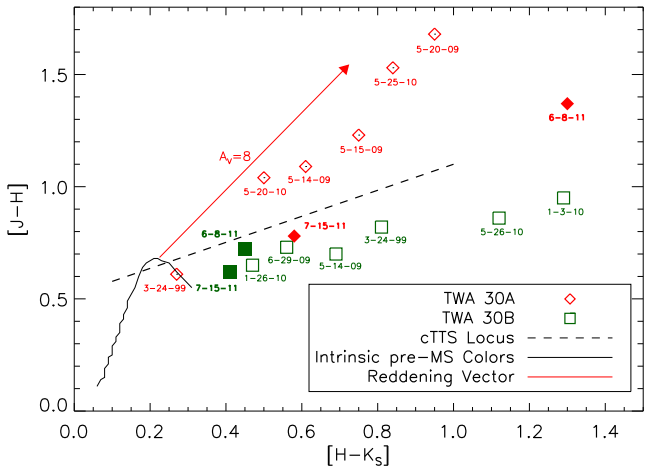


Figure 3. JHK colour–colour plot of the variable TWA 30A (red diamonds) and 30B (green squares). A selection of photometry extracted from spectral observations between 1999 and 2010, and initially, presented in Looper et al. (2010a) are shown with unfilled symbols. Photometry extracted from IRTF SpeX and VLT spectral observations in 2011 are shown with filled symbols. The intrinsic pre-MS colours of ∼5–30 Myr old stars are shown in black (Pecaut & Mamajek 2013). The classical T Tauri star locus (Meyer, Calvet & Hillenbrand 1997) and a reddening vector corresponding to an $A_V = 8$ are shown in black (dashed) and red (solid) lines, respectively.

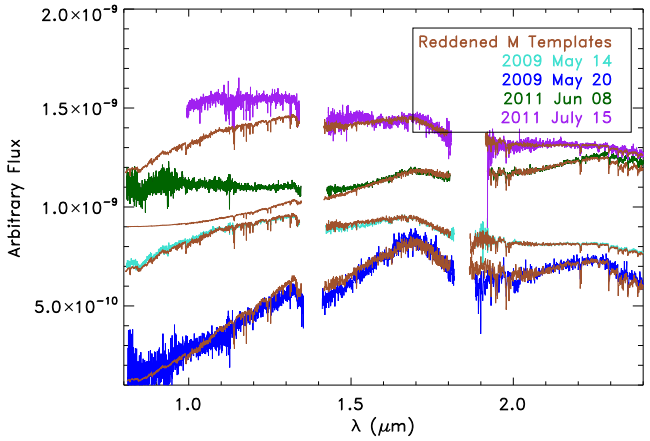


Figure 4. A comparison between a selection of extincted SpeX observations of TWA 30A presented in Looper et al. (2010a, blue and teal) and this work (green and purple). All spectra were fit with reddened M templates ($R_V = 3.1$; M5 for epochs 2009 May 14 and 2011 July 11 and M6 for 2009 May 20 and 2011, June 8) with corresponding reddening values of $A_V = 4.65$, 4.7, 9.0, and 14.9, respectively. Each spectrum was normalized to its corresponding spectral template at ∼2.15 μm. A previously unobserved excess is clearly visible in the 2011 June and July epochs. Spectra from top to bottom at 1.5 μm (with coincident reddened templates) are 2011 July 15, 2011 Jun 8, 2009 May 14, and 2009 May 20.

within each filter bandpass.[2] In Fig. 3, the 2011 June/July effective 2MASS colours are shown in a near-IR colour–colour diagram and compared to a selection of data presented in Looper et al. (2010b). In the case of TWA 30A, Figs 3 and 4 demonstrate a large variability in extinction and a previously unobserved near-IR excess (∼0.8–1.6 μm). Due to the near-IR excess apparent in the data presented here, we choose not to derive L_{bol} from *J*-band photometry and instead adopt the previously derived $\log(L_{bol}/L_\odot) = -1.70$ from Looper et al. (2010a) with the assumption that L_{bol} has not changed considerably between the two epochs. TWA 30B displays levels of near-IR excess near or below the minimum previously reported.

[2] The near-IR spectroscopy results presented in this work will be limited to calculations involving extinction and continuum shape. Detailed UVB-NIR line analyses will be presented in a future paper by B. Stelzer.

Table 2. *J H K* colours and extinction.

Object	Obs. date	(*J*–*H*)	(*H*–*K*)	(J–K)	A_V[a]
TWA 30A	2011-06-08	1.37	1.3	2.67	$14.9^{+0.6}_{-1.3}$
TWA 30A	2011-07-15	0.78	0.58	1.36	$4.7^{+0.6}_{-0.6}$
TWA 30B	2011-06-08	0.72	0.45	1.17	–
TWA 30B	2011-07-15	0.62	0.41	1.03	–

[a]Measured using reddened template spectra with $R_V = 3.1$.

Optical extinction (A_V) was measured for TWA 30A following the same procedure described in Looper et al. (2010a): i.e. spectral templates were reddened according to the reddening curve presented in Cardelli, Clayton & Mathis (1989) with $R_V = 3.1$, and the resulting reddened template spectra were then compared by eye to the observed spectra so as to estimate the best match in terms of both A_V and spectral type. We spectroscopically classified TWA 30A for each observation with the following spectral templates originally used in Looper et al. (2010a) from the IRTF Spectral Library (Cushing, Rayner & Vacca 2005; Rayner, Cushing & Vacca 2009): Gl 213 (M4 V), Gl 51 (M5 V), and Gl 406 (M6 V). The best match to the 2011 June observation of TWA 30A was provided by the M6 spectral template with an extinction correction of $A_V = 14.9$. The best match to the 2011 July observation was provided by the M5 spectral template with an extinction correction of $A_V = 4.7$ (Fig. 4).

Extinction and errors were estimated for TWA 30A by adjusting the reddening (A_V) of the template to obtain the best visual match to the spectrum in the 1.6–2.0 μm wavelength region. The observed spectra did not match the spectral templates at wavelengths $\lesssim$1.6μm, with the comparison indicating the presence of a continuum excess in this wavelength range (Fig. 4). Therefore, measurements of A_V presented here assume that the 1.6–2.0 μm wavelength region is relatively excess-free. This assumption is supported by evidence in that this part of the spectrum fits the reddened spectral templates well in both the 2011 June and July observations and none of the previous eight near-IR observations of TWA 30A presented in Looper et al. (2010a) display an excess at this wavelength. In order to consider dust size distributions different from that of the interstellar medium (ISM), we also determined extinction assuming (ISM-like and non-ISM-like) values of $R_V = 2.75$ and 5.3. For these values of R_V, we find, respectively, estimated optical extinction (A_V) values of 17.3 and 12.7 for the June epoch, and values of 5.1 and 3.7 for the July epoch.

The best match to the TWA 30B spectra was provided by the M4 spectral template (Fig. 2). The spectral types for TWA 30A and 30B determined in this work are consistent with those previously reported in Looper et al. (2010a,b). No values of A_V were calculated for TWA 30B because variability in this system is likely due to near-IR excess and not photospheric extinction (Looper et al. 2010b). The *JHK* colours and measured values of A_V for TWA 30A and *JHK* colours for TWA 30B are listed for the 2011 June and July epochs in Table 2. The optical extinction measured from the 2011 June epoch ($A_V = 4.7$), for TWA 30A is consistent with the 2009 May 14–15 measurements reported in Looper et al. (2010a). Our measured

Downloaded from https://academic.oup.com/mnras/article-abstract/459/2/2097/2595075 by guest on 21 April 2020

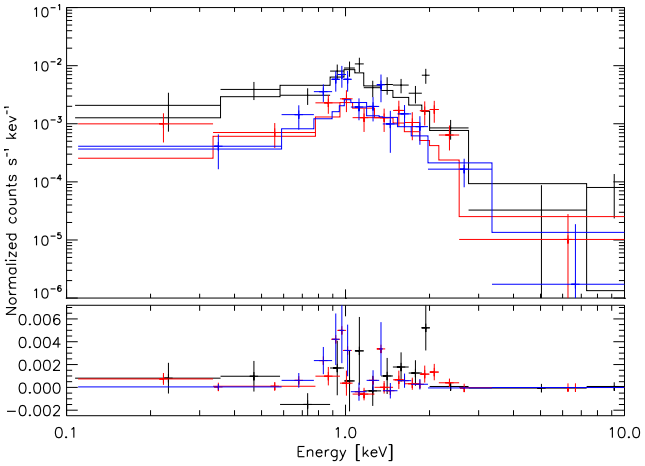


Figure 5. The 2011 July X-ray spectrum of TWA 30A (crosses) fit with an absorbed one-temperature thermal plasma model (histogram). Each colour (black, blue, and red) represents the same model fit to data from each of the *XMM–Newton* EPIC detectors (pn, MOS1, and MOS2), respectively.

extinction for the 2011 June epoch (A_V = 14.9) is significantly higher than the highest extinction previously reported (A_V = 9.0 in 2009 May 20; Looper et al. 2010a).

3.2 X-ray Properties of TWA 30A and 30B

X-ray spectra of TWA 30A from the two *XMM–Newton* observations were extracted and fit with an absorbed, single-temperature thermal plasma emission model (apec) assuming a solar abundance of 0.2 using XSPEC.[3] The metallicity of 0.2 solar was adopted for consistency with previous spectral fitting of XMM data for the M2.5 pre-MS star TWA 11B (López-Santiago et al. 2007). The free parameters of the fit were model normalization (proportional to the emission measure), X-ray plasma temperature (T_X), and neutral hydrogen absorbing column (N_H). The absorbed X-ray flux (F_X) was determined from the best-fitting model (red, χ^2 = 1.42 and 0.92 for the 2011 June and July epochs, respectively). An intrinsic (i.e. unabsorbed) X-ray luminosity (L_X) was calculated using the best-fitting model assuming N_H=0 and a distance of 42 pc (Looper et al. 2010b). The resulting X-ray spectral fit parameters for TWA 30A between 0.15 and 10.0 keV are listed in Table 3. We find no evidence of excess soft ($\lesssim$1 keV) X-ray emission indicative of shocked-heated plasma – such as would be expected given the presence of accretion shocks or shocks in the acceleration region of a jet – at either observing epoch. The 2011 July X-ray spectrum of TWA 30A and best-fitting model is shown in Fig. 5. An attempt to better constrain the X-ray flux near 1 keV was made assuming Ne and Fe abundances similar to those determined in the case of TW Hya (Ne = 2.5, Fe = 0.2; Brickhouse et al. 2010). However, such a model does not improve the fit and yields similar values for the X-ray temperature, absorbing column, and luminosity. Hence, we report the results of the fit to the 0.2 solar abundance apec model (Table 3).

The 2011 June TWA 30A X-ray EPIC-pn spectral fit suffered from large and unconstrained errors in the fit parameters (e.g. kT and F_X) due to a low count rate and particle flaring contamination, which reduced the effective exposure time. The 2011 July X-ray spectral fit is better constrained. X-ray light curves were also constructed for TWA 30A using the 2011 July data, to search for short-time-scale X-ray variability (Fig. 6). Low levels of flaring can be seen in TWA 30A (e.g. increase in count rate by factor of ∼2). X-ray variability between the 2011 June and July epochs is not discussed due to the poorly constrained plasma temperature in the 2011 June epoch.

As reported in the RASS Faint Source Catalogue and Looper et al. (2010a), TWA 30A was detected with *ROSAT* in 1990 with a count rate of (2.5 ± 1.0) × 10^{-2} counts s^{-1}. We estimate the 0.1–2.0 keV intrinsic X-ray luminosity associated with the *ROSAT* count rate using HEASARC PIMMS[4] assuming the same spectral parameters (e.g. kT and N_H) determined from the *XMM–Newton* best-fitting models. We estimate two values of intrinsic L_X for the 1990 RASS observation corresponding to the high-extinction and low-extinction states observed in 2011 June and July, respectively (Table 3). These parameters result in a *ROSAT* intrinsic (i.e. unabsorbed) X-ray luminosity of 5.2 × 10^{29} and 1.4 × 10^{29} erg s^{-1}, respectively. These values of L_X differ significantly from those derived from the same count rate and reported in Looper et al. (2010a, L_X = 4.0 × 10^{28} erg s^{-1}) because they report an X-ray luminosity estimated from the *ROSAT* count rate with a method derived for main sequence low-mass dwarf stars within 7 pc of the Earth (i.e. sources with negligible ISM and no circumstellar absorption; Schmitt, Fleming & Giampapa 1995). Therefore, their calculation does not consider the effects of absorption from circumstellar material which, in the case of a nearly edge-on disc like TWA 30A, can be significant (Table 3). Thus, we adopt our estimated values of *ROSAT* L_X. In order to compare the 2011 June/July XMM observations with that of *ROSAT*, we recalculate the intrinsic X-ray luminosities in the 0.15–2.0 keV energy bandpass. We derive 0.15–2.0 keV X-ray luminosities of L_X = 5.3 × 10^{27} and L_X = 6.2 × 10^{27} erg s^{-1} for the 2011 June and July *XMM* data, respectively. We conclude that the 0.15–2.0 keV X-ray luminosity of TWA 30A decreased by a factor of ∼20–100, where the precise factor decrease depends on the value of N_H assumed for the 1990 (*ROSAT*) data.

TWA 30B was not detected with *XMM–Newton* in either observation; the upper-limit on its pn count rate is estimated to be $\lesssim$1.6 × 10^{-3} s^{-1} for the 2011 July epoch. Assuming D = 44 pc and the same X-ray spectral fit parameters as determined for TWA 30A in its high-extinction state in 2011 June (Table 3), we determine an upper limit on the X-ray luminosity of TWA 30B of $L_X \lesssim$ 3.0 × 10^{27} erg s^{-1}.

4 DISCUSSION

4.1 Near-IR and X-ray variability

Looper et al. (2010a,b) had previously shown, based on near-IR spectroscopy collected over the period 2008–09, that TWA 30A and 30B are highly near-IR variable on time-scales of days and that their variations follow the reddening vector and the cTTS (dust emission excess) locus, respectively. For TWA 30A, this variable emission was suggested to be due to variable obscuration of the stellar photosphere by circumstellar dust. This explanation can account for the variable reddening detected. However, in the observations presented in this work, reddening of the photosphere alone cannot account for TWA 30A's variability. Instead, our measurements of [*J*–*H*] and [*H*–*K*] colours (Fig. 3) evidently display a combination of both reddening and ∼0.8–1.6 μm near-IR excess. Furthermore, the slope of the continuum between ∼0.8 and 1.6 μm is flatter in

[3] http://heasarc.gsfc.nasa.gov/xanadu/xspec/

[4] https://heasarc.gsfc.nasa.gov/cgi-bin/Tools/w3pimms/w3pimms.pl

Downloaded from https://academic.oup.com/mnras/article-abstract/459/2/2097/2595075 by guest on 21 April 2020

Table 3. X-ray spectral fit parameters for TWA 30A.

Obs. date UTC	Count rate (ks^{-1})	pn exp. time (ks^{-1})	N_H (1×10^{22} cm^{-2})	kT (keV)	Norm. $\times 10^{-5}$	Absorbed F_X (erg cm^{-2} s^{-1})	Intrinsic L_X[a] 0.15–10.0 keV (erg s^{-1})
2011-06-08	5.1 ± 1.8[b]	14.0	$0.95^{+1.75}_{-0.61}$	2.22[c]	$4.19^{+2.76}_{-1.70}$	5.59E-14$^{+1.80E-14}$[c]	1.7E+28
2011-07-15	11 ± 1.2	14.7	$0.16^{+0.10}_{-0.06}$	$1.6^{+0.30}_{-0.25}$	$3.43^{+0.83}_{-0.66}$	2.20E-14$^{+3.6E-15}_{-2.9E-15}$	7.9E+27

[a]See Section 3.2 for 0.15–2.0 keV Intrinsic L_X during the 2011 June/July epochs for comparison with the *ROSAT* 1990 detection.
[b]X-ray spectral fitting for 2011 June was performed using only the EPIC-pn detector.
[c]Poorly constrained parameter due to low number of counts.

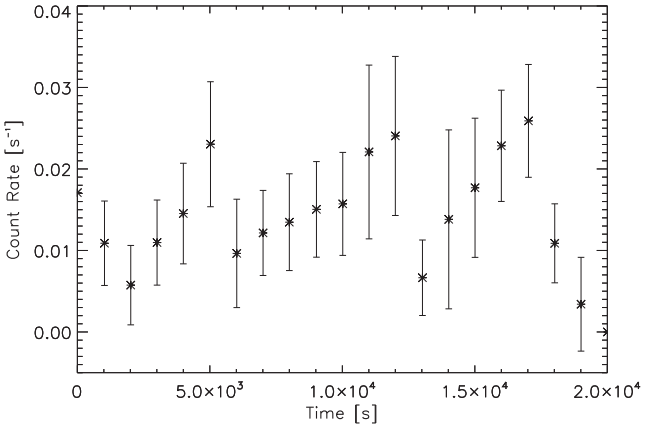


Figure 6. The 2011 July *XMM–Newton* X-ray light curve of TWA 30A with one sigma error bars.

the 2011 June and July observations compared with those of the Looper et al. (2010b) observations, possibly indicative of an additional dust scattering component or a continuum excess (Fig. 4). In the case of classical T Tauri stars, near-IR continuum excess is generally indicative of accretion Hartigan & Kenyon (2003). In the case of TWA 30A, however, accretion is unlikely to contribute excess flux in the 1.6–2.0 μm region where our reddened spectral template fits assume an excess-free region (Section 3.1). We caution that strong accretion signatures, including veiling affecting the Li I and K I lines, have been previously observed in TWA 30A (Looper et al. 2010a), and in some cases, cTTSs have demonstrated NIR continuum excess in the entire ∼0.48–2.1 μm range (Fischer et al. 2011). None the less, the presence of a slight 2.2–2.4 μm excess in the 2011 June observation indicates that excess near-IR continuum emission alone cannot account for the shape of this spectrum. Both the 2011 June and July near-IR spectral observations of TWA 30B closely match the colours and spectral shape of the previous (Looper et al. 2010b) observations obtained at the lowest levels of near-IR excess (Figs 2 and 3).

In the case of TWA 30A, a potential decrease of 1–2 orders of magnitude in L_X over two decades is evident when comparing the results of the 1990 *ROSAT* and 2011 XMM observations (Section 3.2). The physical mechanism by which a pre-MS star can decrease in X-ray luminosity by such significant levels within a timespan of ∼20 yr is unclear. One possibility is that TWA 30A was undergoing a flaring event in 1990. While individual flaring events for pre-MS stars may happen on time-scales of hours to days (e.g. Getman et al. 2005; Favata et al. 2005; Stelzer et al. 2007), longer term (year-time-scale) X-ray variability in count rate has been observed for pre-MS stars in L1630 (e.g. Principe et al. 2014). Another possibility is that TWA 30A may have undergone an accretion outburst similar to those seen in FU Ori and EX Lupi type objects (for a review; see Audard et al. 2014). Such outbursts can be accompanied by order of magnitude changes in brightness in the near-IR, optical and X-ray, as in the case of V1647 Ori (Kastner et al. 2006). However, this scenario cannot be confirmed in the case of TWA 30A as there are no optical/IR observations available contemporaneous with the 1990 *ROSAT* observation. While the mechanism by which TWA 30A has decreased in L_X remains unclear, the impact of such a change in L_X may be significant when considering processes such as disc ionization (Gorti & Hollenbach 2009; Cleeves et al. 2015) and mass loss via X-ray induced photodissociation (Owen, Clarke & Ercolano 2012) over the lifetime of the disc.

In the context of other pre-MS stars of similar mass (∼0.1 $M_\odot$), the intrinsic X-ray luminosity of TWA 30A as measured by *ROSAT* in 1990 appears typical when compared to, e.g. low-mass stars in the ONC (Preibisch & Feigelson 2005) and IC 348 (Stelzer et al. 2012). However, it then follows that the significant decrease in L_X from 1990 to 2011 places TWA 30A well below typical X-ray luminosities for low-mass, pre-MS M-type stars. An important difference to consider when comparing TWA 30A with stars of similar spectral type in the ONC and IC 348 is stellar age and evolution. While TWA 30A may still host a circumstellar disc with signatures of youth, its age (∼8 Myr) is markedly older than its counterparts in the ONC and IC 348 (mean age of 1–2 and 2–3 Myr, respectively; Hillenbrand 1997; Stelzer et al. 2012). Moreover, with a spectral type of M5/M6 (see Section 3) and age of ∼8 Myr, TWA 30A lies very close to the substellar boundary as indicated by its HR diagram position given pre-MS stellar evolution models of Baraffe et al. (1998) and D'Antona & Mazzitelli (1997, e.g. see figs 5 and 1 in Luhman et al. 2003 and Preibisch et al. 2005 for HR diagrams and evolutionary models of pre-MS stars in Taurus and pre-MS brown dwarfs in the ONC, respectively) . Such models indicate an M5/M6 star at ∼8 Myr may have evolved from and will evolve to a later spectral type (∼M7, i.e. the substellar boundary). Indeed, while the X-ray luminosity of TWA 30A is lower than its ∼M5 counterparts in IC 348 (Stelzer et al. 2012), it is consistent with those of the ∼1 Myr ONC ∼M7 brown dwarfs (Preibisch et al. 2005).

Fractional X-ray luminosity is a commonly used proxy for magnetic activity in young stars (e.g. Grosso et al. 2007). TWA 30A's fractional X-ray luminosity in the 2011 July epoch (L_X/L_{bol} ∼1.0 × 10^{-4}) was lower than many of the reported ∼M5–M7 pre-MS stars in the ONC, Taurus, and IC 348 (Grosso et al. 2007; Güdel et al. 2007; Stelzer et al. 2012), while its intrinsic L_X is significantly fainter than its similar-massed counterparts. If these values are representative of TWA 30A's quiescent state, the low L_X/L_{bol} and L_X values suggest that TWA 30A may be a representative of the progenitors of the late-type M and early L-type main-sequence dwarf stars which display a lack of X-rays (Berger 2006; Berger et al. 2010). In the case of main sequence stars, such phenomena may be the result of changes in magnetic field configuration or the decreasing ionization fractions in the stellar atmosphere (Mohanty et al. 2002; Berger 2006). A smaller ionization fraction in the stellar atmosphere

Downloaded from https://academic.oup.com/mnras/article-abstract/459/2/2097/2595075 by guest on 21 April 2020

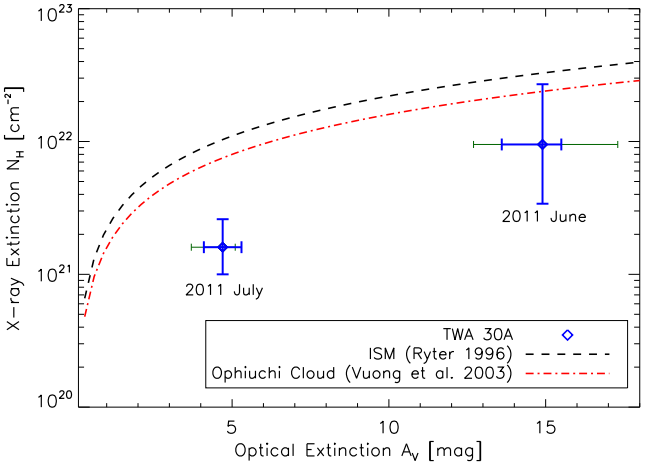


Figure 7. The relationship between gas ($N_{\rm H}$) and dust ($A_{\rm V}$) extinction in TWA 30A for two epochs of contemporaneous observations compared to the ISM (black dashed line; Ryter 1996) and the ρ Ophiuchi molecular cloud (red dash-dotted line; Vuong et al. 2003), all of which assume that an $R_{\rm V}$ = 3.1. For each observation, the uncertainty in the determinations of $A_{\rm V}$ corresponding to a plausible range of $R_{\rm V}$ for dust in the TWA 30A disc (i.e. $R_{\rm V}$ = 2.75 to 5.3; see Sections 3.1, 4.2) is shown as a green error bar.

will decrease the coupling of that material to the stellar magnetic fields, and thus, will decrease the coronal X-ray luminosity. With a spectral type of M5/M6, TWA 30A ($T_{\rm eff}$ ∼3050; Luhman et al. 2003) lies at the border of the regime ($T_{\rm eff}$ of 1500–3000) investigated in Mohanty et al. (2002) for main-sequence mid-M to late-L stars, where magnetic interaction (between the chromosphere and stellar magnetic field) was limited.

It also follows that TWA 30B, with an upper limit of $L_{\rm X} < 3.0 \times 10^{27}$ erg s^{-1} appears unusually X-ray faint compared to similar stars in the ONC, Taurus and IC 348. Specifically, given a spectral type of ∼M4 and an age of ∼8 Myr, we estimate the fractional X-ray luminosity of TWA 30B of $L_{\rm X}/L_{bol} < 1.5 \times 10^{-5}$ (Luhman et al. 2003), a value well below that of its similar mass counterparts in other nearby star-forming regions. Additional X-ray observations of pre-MS mid-M stars (e.g. pre-MS stars that will evolve into main-sequence M7 and early L dwarfs) are needed to better understand whether such a decrease in magnetic activity as probed by $L_{\rm X}/L_{\rm bol}$ is characteristic of these young low-mass stars near the H-burning limit. TWA 30A and 30B appear to be at the cusp of this X-ray active/inactive boundary. This suggests that, in this binary, we could be seeing the 'turn-off' of X-ray activity in pre-MS low-mass stars that is observed in main sequence stars of type ∼M7 or later.

While optical evidence suggests TWA 30A is actively accreting (Looper et al. 2010b), we find no evidence of shock-heated plasma at temperatures characteristic of free-fall accretion on to a mid-M-type pre-MS star (T ∼ 2 MK; Brickhouse et al. 2010, and references therein). This suggests that the hydrogen absorbing column density ($N_{\rm H}$) is too large, and/or the emission measure of shocked material is too small to detect such an X-ray accretion signature. To probe shocks at the base of a jet, i.e. shocks farther from the star and thus more difficult to hide behind an absorbing disc, higher resolution X-ray observations are needed.

4.2 Relationship between atomic and optical extinction

A comparison of measurements of $N_{\rm H}$ and $A_{\rm V}$ for TWA 30A at our two observing epochs (see Tables 2 and 3) is shown in Fig. 7. These results are overlaid with $N_{\rm H}$ versus $A_{\rm V}$ curves determined for the ISM (Ryter 1996) and ρ Ophiuchi molecular cloud gas (Vuong et al. 2003). Regardless of the choice of $R_{\rm V}$ assumed in our calculation of $A_{\rm V}$, a correlation between optical and X-ray extinction is evident for TWA 30A: both $A_{\rm V}$ and $N_{\rm H}$ are found to decrease between 2011 June to July. Such variability is consistent with variable obscuration of the photosphere by a disc warp and/or clump. Other pre-MS star–disc systems notable for their high disc inclinations show similar levels of optical variability (e.g. AA Tau; RY Lupi; T Cha; Grosso et al. 2007; Manset et al. 2009; Schisano et al. 2009), although no correlated X-ray absorption has yet been detected with contemporaneous observations.

In the case of TWA 30A, an estimate of the warp/clump mass can be made from the X-ray spectral fitting results if we assume that this material completely covers the photosphere of the star during the 2011 June observation and does not cover the photosphere during the 2011 July observations. The clump column density can then be estimated as the difference between the 2011 June and July observations (7.9×10^{21} cm^{-2}). The clump mass is then $M_{\rm cl} = N_{\rm H} \times \pi \times R_*^2 \times m_{\rm H}$. Using the effective temperature, bolometric luminosity of TWA 30A (∼3050 K and 7.6×10^{31} erg s^{-1}) and the Stefan–Boltzmann law, we estimate the radius of TWA 30A to be R_* ∼0.5 R$_\odot$. We hence infer a clump mass of $M_{\rm cl} \approx 5.0 \times 10^{19}$ g or $8.4 \times 10^{-9} M_\oplus$. A similar estimate was made for a disc clump in T Cha, for which Schisano et al. (2009) report a clump mass $M_{\rm cl} \approx 4 \times 10^{20} g$. However, their calculation was based on optical extinction ($A_{\rm V}$) and an assumed $N_{\rm H}$ to $A_{\rm V}$ relationship. For comparison, the mass of the Martian moon Phobos is 1.06×10^{19} g (Pätzold et al. 2014).

Independent measurements of $N_{\rm H}$ and $A_{\rm V}$ can be used to determine the ratio of atomic absorption from gas and optical extinction due to dust (e.g. Sacco et al. 2014). Comparing these values as determined for the nearly edge-on circumstellar disc of TWA 30A with those typical of the ISM (Fig. 7) can help constrain the chemical environment in which planets might form. In this respect, it is intriguing that the apparent correlated changes in $N_{\rm H}$ and $A_{\rm V}$ we find for the TWA 30A disc follow the trend of increasing $N_{\rm H}$ with increasing $A_{\rm V}$ displayed in Fig. 7 for the ISM and stars in ρ Oph. However, even considering different values of $R_{\rm V}$, at both epochs TWA 30A lies below the line typical of that of the ISM, indicating a deficiency of the metals (C, N, and/or O) that are most responsible for soft X-ray absorption. This suggests that either these metals are not abundant in the gas component of the TWA 30A disc, or that these metals are frozen out as molecular (e.g. CO, CO_2, and CH_4) ices on to dust grains, reducing their X-ray absorption cross-sections. Such molecular gas freeze-out has long been inferred in T Tauri star circumstellar discs (e.g. Dutrey, Guilloteau & Guelin 1997) at radii larger than the 'snow line' (freeze-out radius) for each chemical species. Recent observations have confirmed the presence of such a snow line, for CO, within the disc orbiting TW Hya (Qi et al. 2013). However, we caution that the $N_{\rm H}/A_{\rm V}$ values typical of that of the ISM depend on dust grain properties that are not necessarily characteristic of the TWA 30A disc. Furthermore, standard X-ray absorbing models assume conditions similar to that of the ISM, where only ∼20 per cent of available gas is in molecular form (Wilms et al. 2000). In circumstellar discs, the percentage of gas in molecular form is likely to be far higher, and as noted, the gas phase metals may be depleted.

5 SUMMARY

We have used contemporaneous multiwavelength observations to study two of the nearest known examples of actively accreting,

Downloaded from https://academic.oup.com/mnras/article-abstract/459/2/2097/2595075 by guest on 21 April 2020

pre-MS star systems, TWA 30A and 30B. These two stars have masses near the substellar boundary and are orbited by circumstellar discs viewed nearly edge-on, with evidence for collimated stellar outflows. Both TWA 30A and 30B have previously displayed highly variable near-IR variability on time-scales of hours to days. We obtained and analysed two epochs of *XMM–Newton* X-ray observations contemporaneous with VLT XSHOOTER and IRTF SpeX spectra to investigate variability, magnetic activity, and the composition of circumstellar disc material associated with TWA 30A and 30B.

We measure TWA 30A at both high and low levels of extinction ($A_V = 14.9$ and 4.7). While the lower level of extinction is consistent with previous measurements, the highest extinction we measure is several magnitudes higher than previously reported. We also report a previously unobserved near-IR excess during both 2011 June and July epochs. For TWA30B, we measure variable near-IR excesses that are consistent with the low end of the range measured in previous studies. From X-ray spectral fitting of TWA 30A, we find intrinsic 0.15–10.0 keV X-ray luminosities of $\sim 2 \times 10^{28}$ and $\sim 8 \times 10^{27}$ erg s^{-1} in 2011 June and July, respectively, and column densities of $N_H \sim 1 \times 10^{22}$ and $N_H \sim 2 \times 10^{21}$ cm^{-2}, respectively. The 0.15–2.0 keV X-ray luminosities of TWA 30A display a factor of 20–100 decrease relative to a 1990 *ROSAT* X-ray detection. TWA 30B was not detected by *XMM–Newton,* and an upper limit of $L_X < 3.0 \times 10^{27}$ erg s^{-1} was estimated. Magnetic activity, as probed by $\log(L_X/L_{bol})$, is measured for TWA 30A from the 2011 July epoch (~ -4.0) and estimated for TWA 30B (≤ -4.8); in both cases the values of L_X/L_{bol} are lower than many of the young pre-MS stars of similar mass in the ONC, Taurus and IC 348. Combined with their very faint intrinsic X-ray luminosities, this suggests that, in the TWA 30 binary, we could be seeing the onset of the decline in ultralow-mass star X-ray activity that is observed in main-sequence stars of ∼M7 or later. No soft X-ray excess indicative of emission due to shocks, resulting from accretion or jet activity, was detected.

Near-IR spectra were analysed to estimate disc dust extinction and, combined with *XMM–Newton* spectra, to measure the ratio of N_H/A_V in the circumstellar disc of TWA 30A. We find that variations in optical/IR extinction due to dust and X-ray absorption due to gas appear to be correlated. We estimate the mass obscuring the photosphere during the 2011 June observation to be $M_{cl} \approx 5.0 \times 10^{19} g$. Assuming an $R_V = 3.1$, we measure N_H to A_V ratios of $\sim 3 \times 10^{20}$ and $\sim 6 \times 10^{20}$ mag^{-1}cm^{-2} for observations during low- and high-extinction states, respectively. These values are lower than those typical of the ISM, suggesting that the circumstellar disc metals responsible for absorbing X-rays are either not present or are frozen out on to dust grains.

ACKNOWLEDGEMENTS

We thank D. Looper for providing IRTF observations of TWA 30, the ESO Director for providing DDT XSHOOTER observations of TWA 30A and 30B, and R. Montez Jr and V. Rapson for helpful suggestions during the data reduction process. This research was supported in part by grants to RIT from the NASA GSFC *XMM–Newton* Guest Observer Facility (award NNX12AB63G), the National Science Foundation (award AST–1108950), and the NASA Astrophysics Data Analysis Program (award NNX12AH37G). DP acknowledges a CONICYT-FONDECYT award (grant 3150550); and the Millennium Science Initiative (Chilean Ministry of Economy; grant Nucleus RC 130007).

REFERENCES

Alcalá J. M. et al., 2014, A&A, 561, A2
Audard M. et al., 2014, in Beuther H., Klessen R. S., Dullemond C. P., Henning T. eds., Protostars and Planets VI. Univ. Arizona Press, Tucson, p. 387
Baraffe I., Chabrier G., Allard F., Hauschildt P. H., 1998, A&A, 337, 403
Berger E., 2006, ApJ, 648, 629
Berger E. et al., 2010, ApJ, 709, 332
Bouvier J. et al., 2003, A&A, 409, 169
Bouvier J., Alencar S. H. P., Harries T. J., Johns-Krull C. M., Romanova M. M., 2007, in Reipurth B., Jewitt D., Keil K., eds., Protostars and Planets V. Univ. Arizona Press, Tucson, AZ, p. 479
Brickhouse N. S., Cranmer S. R., Dupree A. K., Luna G. J. M., Wolk S., 2010, ApJ, 710, 1835
Cardelli J. A., Clayton G. C., Mathis J. S., 1989, ApJ, 345, 245
Chadney J. M., Galand M., Unruh Y. C., Koskinen T. T., Sanz-Forcada J., 2015, Icarus, 250, 357
Ciesla F. J., 2007, Science, 318, 613
Cleeves L. I., Bergin E. A., Qi C., Adams F. C., Öberg K. I., 2015, ApJ, 799, 204
Cohen M., Wheaton W. A., Megeath S. T., 2003, AJ, 126, 1090
Cushing M. C., Rayner J. T., Vacca W. D., 2005, ApJ, 623, 1115
D'Antona F., Mazzitelli I., 1997, Mem. Soc. Astron. Ital., 68, 807
Ducourant C., Teixeira R., Galli P. A. B., Le Campion J. F., Krone-Martins A., Zuckerman B., Chauvin G., Song I., 2014, A&A, 563, A121
Dutrey A., Guilloteau S., Guelin M., 1997, A&A, 317, L55
Favata F., Flaccomio E., Reale F., Micela G., Sciortino S., Shang H., Stassun K. G., Feigelson E. D., 2005, ApJS, 160, 469
Fischer W., Edwards S., Hillenbrand L., Kwan J., 2011, ApJ, 730, 73
Flaherty K. M., Muzerolle J., 2010, ApJ, 719, 1733
Getman K. V. et al., 2005, ApJS, 160, 319
Glassgold A. E., Galli D., Padovani M., 2012, ApJ, 756, 157
Gorti U., Hollenbach D., 2009, ApJ, 690, 1539
Gorti U., Hollenbach D., Dullemond C. P., 2015, ApJ, 804, 29
Grosso N., Bouvier J., Montmerle T., Fernández M., Grankin K., Zapatero Osorio M. R., 2007, A&A, 475, 607
Güdel M. et al., 2007, A&A, 468, 353
Hartigan P., Kenyon S. J., 2003, ApJ, 583, 334
Hillenbrand L. A., 1997, AJ, 113, 1733
Huenemoerder D. P., Kastner J. H., Testa P., Schulz N. S., Weintraub D. A., 2007, ApJ, 671, 592
Jayawardhana R., Hartmann L., Fazio G., Fisher R. S., Telesco C. M., Piña R. K., 1999, ApJ, 520, L41
Kastner J. H., Zuckerman B., Weintraub D. A., Forveille T., 1997, Science, 277, 67
Kastner J. H., Huenemoerder D. P., Schulz N. S., Canizares C. R., Weintraub D. A., 2002, ApJ, 567, 434
Kastner J. H. et al., 2006, ApJ, 648, L43
Koenigl A., 1991, ApJ, 370, L39
Krist J. E., Stapelfeldt K. R., Ménard F., Padgett D. L., Burrows C. J., 2000, ApJ, 538, 793
Lammer H., Selsis F., Ribas I., Guinan E. F., Bauer S. J., Weiss W. W., 2003, ApJ, 598, L121
Lépine S., Hilton E. J., Mann A. W., Wilde M., Rojas-Ayala B., Cruz K. L., Gaidos E., 2013, AJ, 145, 102
Looper D. L., Bochanski J. J., Burgasser A. J., Mohanty S., Mamajek E. E., Faherty J. K., West A. A., Pitts M. A., 2010a, AJ, 140, 1486
Looper D. L. et al., 2010b, ApJ, 714, 45
López-Santiago J., Micela G., Sciortino S., Favata F., Caccianiga A., Della Ceca R., Severgnini P., Braito V., 2007, A&A, 463, 165
Lubow S. H., D'Angelo G., 2006, ApJ, 641, 526
Luhman K. L., Briceño C., Stauffer J. R., Hartmann L., Barrado y Navascués D., Caldwell N., 2003, ApJ, 590, 348
Mamajek E. E., Meyer M. R., Liebert J., 2002, AJ, 124, 1670
Manset N., Bastien P., Ménard F., Bertout C., Le van Suu A., Boivin L., 2009, A&A, 499, 137

Downloaded from https://academic.oup.com/mnras/article-abstract/459/2/2097/2595075 by guest on 21 April 2020

Meijerink R., Aresu G., Kamp I., Spaans M., Thi W.-F., Woitke P., 2012, A&A, 547, A68
Meyer M. R., Calvet N., Hillenbrand L. A., 1997, AJ, 114, 288
Mohanty S., Basri G., Shu F., Allard F., Chabrier G., 2002, ApJ, 571, 469
Owen J. E., Clarke C. J., Ercolano B., 2012, MNRAS, 422, 1880
Pätzold M., Andert T. P., Tyler G. L., Asmar S. W., Häusler B., Tellmann S., 2014, Icarus, 229, 92
Pecaut M. J., Mamajek E. E., 2013, ApJS, 208, 9
Preibisch T., Feigelson E. D., 2005, ApJS, 160, 390
Preibisch T. et al., 2005, ApJS, 160, 582
Principe D. A., Kastner J. H., Grosso N., Hamaguchi K., Richmond M., Teets W. K., Weintraub D. A., 2014, ApJS, 213, 4
Qi C. et al., 2013, Science, 341, 630
Rayner J. T., Cushing M. C., Vacca W. D., 2009, ApJS, 185, 289
Rodriguez D. R., van der Plas G., Kastner J. H., Schneider A. C., Faherty J. K., Mardones D., Mohanty S., Principe D., 2015, A&A, 582, L5
Ryter C. E., 1996, Ap&SS, 236, 285
Sacco G. G., Kastner J. H., Forveille T., Principe D., Montez R., Zuckerman B., Hily-Blant P., 2014, A&A, 561, A42
Schisano E., Covino E., Alcalá J. M., Esposito M., Gandolfi D., Guenther E. W., 2009, A&A, 501, 1013
Schmitt J. H. M. M., Fleming T. A., Giampapa M. S., 1995, ApJ, 450, 392
Schneider A., Melis C., Song I., 2012, ApJ, 754, 39
Segura A., Kasting J. F., Meadows V., Cohen M., Scalo J., Crisp D., Butler R. A. H., Tinetti G., 2005, Astrobiology, 5, 706
Shu F., Najita J., Ostriker E., Wilkin F., Ruden S., Lizano S., 1994, ApJ, 429, 781
Stelzer B., Flaccomio E., Briggs K., Micela G., Scelsi L., Audard M., Pillitteri I., Güdel M., 2007, A&A, 468, 463
Stelzer B., Preibisch T., Alexander F., Mucciarelli P., Flaccomio E., Micela G., Sciortino S., 2012, A&A, 537, A135
Stelzer B., Marino A., Micela G., López-Santiago J., Liefke C., 2013, MNRAS, 431, 2063
Tarter J. C. et al., 2007, Astrobiology, 7, 30
Vuong M. H., Montmerle T., Grosso N., Feigelson E. D., Verstraete L., Ozawa H., 2003, A&A, 408, 581
Williams J. P., Cieza L. A., 2011, ARA&A, 49, 67
Wilms J., Allen A., McCray R., 2000, ApJ, 542, 914
Zhu Z., Nelson R. P., Dong R., Espaillat C., Hartmann L., 2012, ApJ, 755, 6

This paper has been typeset from a TEX/LATEX file prepared by the author.

Downloaded from https://academic.oup.com/mnras/article-abstract/459/2/2097/2595075 by guest on 21 April 2020